

This is the peer reviewed version of the following article:

Nina Gartner, Tadeja Kosec, Stéphane Poyet, Andraž Legat

The corrosion properties of steel in pore solutions obtained from alkali-activated mortars

Materials and Corrosion

Volume 74

Issue 7

ISSN 0947-5117

which has been published in final form at <https://doi.org/10.1002/maco.202313729>. This article may be used for non-commercial purposes in accordance with Wiley Terms and Conditions for Use of Self-Archived Versions. This article may not be enhanced, enriched or otherwise transformed into a derivative work, without express permission from Wiley or by statutory rights under applicable legislation. Copyright notices must not be removed, obscured or modified. The article must be linked to Wiley's version of record on Wiley Online Library and any embedding, framing or otherwise making available the article or pages thereof by third parties from platforms, services and websites other than Wiley Online Library must be prohibited.

Article type: Research Article

Title: The corrosion properties of steel in pore solutions obtained from alkali-activated mortars

Nina Gartner^{1*}, Tadeja Kosec¹, Stéphane Poyet², Andraž Legat¹

¹ Slovenian National Building and Civil Engineering Institute, Dimičeva ulica 12, 1000 Ljubljana

² Den-SERVICE d'Etude du Comportement des Radionucléides (SECR), CEA, Université Paris-Saclay, F-91191, Gif-sur-Yvette, France

*Correspondence: Nina Gartner, Slovenian National Building and Civil Engineering Institute, Dimičeva ulica 12, 1000 Ljubljana

Email: nina.gartner@zag.si

Abstract

Alkali-activated materials (AAMs) are considered a promising alternative to materials made from ordinary Portland cement (OPC). Other than considering the durability of the material itself, the use of AAMs for reinforced concrete elements also raises the question of steel corrosion processes in these materials, which are still relatively unknown. Three different alkali-activated mortars were prepared for this study, based on either fly ash, slag or metakaolin. Pore solutions were then extracted from each mortar and chemically analyzed. Electrochemical techniques were used to study the corrosion of steel in synthetic pore solutions containing varying concentrations of chlorides. In parallel, the same corrosion tests were performed in a generic pore solution representing OPC mortar. It was shown that the chemical composition differed in each pore solution tested, thus affecting the corrosion properties of the steel. The addition of chloride also had a varying effect on the corrosion properties of the steel in each type of pore solution tested. This study provided a basic overview of the corrosion behaviour and mechanisms of the various AAM environments in comparison to that of OPC.

Keywords: corrosion; alkali-activated materials; extracted pore solution; electrochemical corrosion techniques

1 INTRODUCTION

Concrete is the most widely used engineering material, due to both its relatively low price and its suitability for use in a wide variety of environments. One of the main components of concrete is ordinary Portland cement (OPC), the production of which is estimated to be responsible for 5–8 % of anthropogenic CO₂ emissions worldwide [1,2]. In blended cements OPC is partially replaced by supplementary cementitious materials (SCM), while alkali-activated materials (AAMs) present a potential alternative solution, where alkali-activated aluminosilicate precursors are used as a total replacement for OPC [3,4]. The sustainability of these materials, however, strongly depends on the local availability of SCM (e.g. fly ash, slags, and calcined clays) and optimal use of the alkali activator (e.g. sodium hydroxide) [5]. These materials are not considered as a total replacement for OPC-based concretes, but the wide range of combinations available [3] offers materials with advanced properties for specific applications [6–8].

The use of AAMs for reinforced concrete elements raises the issue of steel corrosion, which is considered to be the main reason for their reduced durability. Carbonation of the concrete and the presence of chloride ions are the main causes of steel corrosion in OPC-based reinforced concrete structures [2].

There are certain differences between the corrosion processes of steel tested in solid cementitious materials (also AAMs) compared to steel exposed solely to their pore solutions. The anodic and cathodic sites in solid materials are spatially localized due to their porous structure [9], while the transport of the electrolyte and oxygen is also affected by the porosity [10]. Pore solutions from AAMs can, however, be significantly different to those derived from

OPC-based concrete mixes, due to differences in their chemical composition, mineralogical properties and redox characteristics [11]. These properties can significantly influence the corrosion processes of steel within AAMs and also make the interpretation of the electrochemical parameters measured more difficult [11].

The aim of this paper is to evaluate the influence of various AAM and OPC pore solutions on steel corrosion and the role of the presence of chloride ions. Various electrochemical and microscopy techniques were used in order to compare the corrosion properties, the type of corrosion and its extent, and the effect of chloride ions in pore solutions from different materials.

2 MATERIALS AND METHODS

The alkali-activated mortars used in this study, from which pore solutions were extracted, were developed by RILEM TC 247-DTA [12–15] and based on three types of precursors: fly-ash (FA8), metakaolin (MK2) and steel slag (S3a-661). The names of the RILEM TC 247-DTA mortar mixes (FA8, MK2 and S3a-661) are used in this study to identify the associated pore solutions. More information regarding the mix design of these mortars are available in our previous work [16]. The cast mortar mixes were cured in sealed plastic foil. After 28 days of curing, the mortar specimens, which were not sufficiently moist, were broken into smaller pieces, 3-4 cm in length, and slowly wetted with distilled water, such that the mortar absorbed all the excess water. After one day of drip-wetting, the pore solutions were extracted from the mortars using a high-pressure device (creating pressures of up to 1000 MPa) [17,18]. Following extraction, the pH and chemical composition of the various pore solutions was analysed using a 940 Professional IC Vario ion exchange chromatography system (Metrohm). Simulated pore solutions were prepared, based on the results (Table 1). The pH was modified by adjusting the ratio of silicate in the OH^- ions. In parallel, a solution of 0.031M NaOH (pH = 12.8) was

prepared, mimicking the pore solution from concrete made of ordinary Portland cement (OPC pore solution).

Table 1. Chemical compositions of the simulated pore solutions, prepared on the basis of analysis of the pore solutions extracted from the three alkali activated mortars (made from fly-ash (FA8), metakaolin (MK2) and steel slag (S3a-661)) [16].

Pore solution type	pH	Salts [g/L]									
		NaCl	KCl	K ₂ SO ₄	Na ₂ SO ₄	NaNO ₃	Na ₂ HPO ₄	NaOH	KOH	Na ₂ Si ₂ O ₅ (72 wt.%)	
AAM	FA8	12.4	0.053	-	1.502	22.871	-	7.859	2.081	-	79.968
	MK2	12.5	0.054	-	0.089	0.275	0.646	-	5.840	-	184.670
	S3a-661	12.7	-	0.400	0.914	-	-	-	1.430	1.805	196.486
OPC	12.8	-	-	-	-	-	-	-	1.240	-	-

The bare simulated pore solutions (Table 1), as well as the same pore solutions with the addition of 0.4 wt. % (0.12 mol/L), 1.0 wt. % (0.29 mol/L) and 2.1 wt. % (0.60 mol/L) concentration of chlorides, were used as the electrolytes for various measurements of electrochemical corrosion. A standard 3-electrode corrosion cell was used to perform the experiments. Carbon steel discs, with a surface area of 0.785 cm² and a similar microstructure and chemical composition to the steel reinforcement used in concrete, were used as the working electrodes (Table 2). The samples were polished before the experiments, using 600 grit SiC paper, and ultrasonically cleaned in ethanol. A graphite electrode served as the counter electrode while a saturated calomel electrode (SCE) or Ag/AgCl electrode was used as the reference electrode. All potential measurements obtained using the Ag/AgCl electrode were re-calculated to the SCE scale (–0.044 V).

Table 2. Chemical composition of the steel working electrode used for the electrochemical measurements.

Carbon (C)	Phosphorus (P)	Sulphur (S)	Copper (Cu)	Nitrogen (N)	Carbon Equivalent (C_{eq})
0.14 wt.%	0.008 wt.%	0.012 wt.%	0.073 wt.%	0.006 wt.%	0.23 wt.%

Selected electrochemical techniques were performed, starting with linear polarisation resistance (LPR) measurements, followed by electrochemical impedance spectroscopy (EIS) and then cyclic potentiodynamic polarisation (CPD) scans. The LPR measurement in AAM pore solutions was performed after 1.5h stabilization in the exposure conditions, while steel in the OPC pore solution required 12h to stabilize. The potential interval of LPR measurements was set from -20 mV to $+20$ mV relative to the open-circuit potential (E_{oc}) measured before the LPR measurement. The scan rate was 0.1 mV/s and the sampling period 1 s. The polarisation potential was scanned via CPD measurements from -0.25 V vs. E_{oc} to $+0.75$ V vs. reference potential (E_{ref}) and back to -0.25 V vs. E_{oc} , using a scan rate of 1 mV/s and a sampling period of 1 s. EIS was measured at open circuit potential (E_{oc}). The frequency range was set between 65 kHz and 5 mHz, with 11 measuring points per decade. The total impedance ($|Z_{total}|$) values were estimated as impedance ($|Z|$) values at the lowest frequencies measured, less the solution resistance (R_s) values.

j_{corr} values were calculated using the Stern-Geary equation presented in Equation 1. Total impedance $|Z_{total}|$ value less the solution resistance (R_s) value were used as a near estimation for polarisation resistance (R_p), and an estimated constant of $B = 0.026$ V [19] was used. v_{corr} values were calculated according to Equation 2 [20], using $AM = 55.85$ as an atomic mass value, a valence of $n = 2$, a Faraday constant of $F = 9.65 \times 10^4$ As, and a steel density value of $\rho = 7.89$ g/cm³.

$$R_p = \frac{B}{j_{corr}} \quad (1)$$

$$v_{\text{corr}} = \frac{AM \cdot j_{\text{corr}}}{n \cdot F \cdot \rho} \quad (2)$$

The steel electrodes (Table 2) were scratched and then immersed in the selected pore solution (Table 1) with and without the addition of Cl^- (at concentrations of 0.4 %, 1.0 %, or 2.1 %). After 27 days of exposure the electrodes were visually analysed and compared.

3 RESULTS AND DISCUSSION

The corrosion studies described in this paper were performed in three different simulated AAM pore solutions and a 0.031M NaOH solution (i.e a simulated OPC pore solution) with a pH of approximately 12.8 (Table 1). Tests were also performed in the same four simulated pore solutions with the addition of Cl^- , to concentrations of 0.4 wt. % (0.12 mol/L), 1.0 wt. % (0.29 mol/L) and 2.1 wt. % (0.60 mol/L).

Linear polarisation (LPR) measurements and polarisation resistance (R_p) values are presented in Figure 1, alongside standard deviations. Small differences in measurements of LPR were observed in the AAM pore solutions without chlorides. The values of polarisation resistance (R_p , Figure 1, Supplement Figure 1) were fairly high and represent average corrosion rates of lower than 1 $\mu\text{m}/\text{year}$. LPR measurements in the pore solutions with the addition of a small concentration of chlorides (0.4 %) showed an increase in R_p values in the FA8 and MK2 solutions. The addition of 1 % Cl^- , however, led to a decrease in R_p values, and consequently an increase in the corrosion rates (v_{corr}) in all the solutions tested, although this was more pronounced in MK2 and S3a-661. The influence of Cl^- on the average corrosion rate was most noticeable in the MK2 pore solution, where the rates were 2.3 \times higher than in the pore solution without chlorides. In the S3a-661 pore solution, the corrosion rate increased up to 1.8 \times , while in the FA8 pore solution the increase in corrosion rate was negligible (1.06 \times higher) when chlorides were added. In general, it was observed that, when chlorides were added to the pore

solutions, there was a more significant reduction in the R_p values in the metakaolin- and slag-based solutions compared to those in the fly-ash based solution.

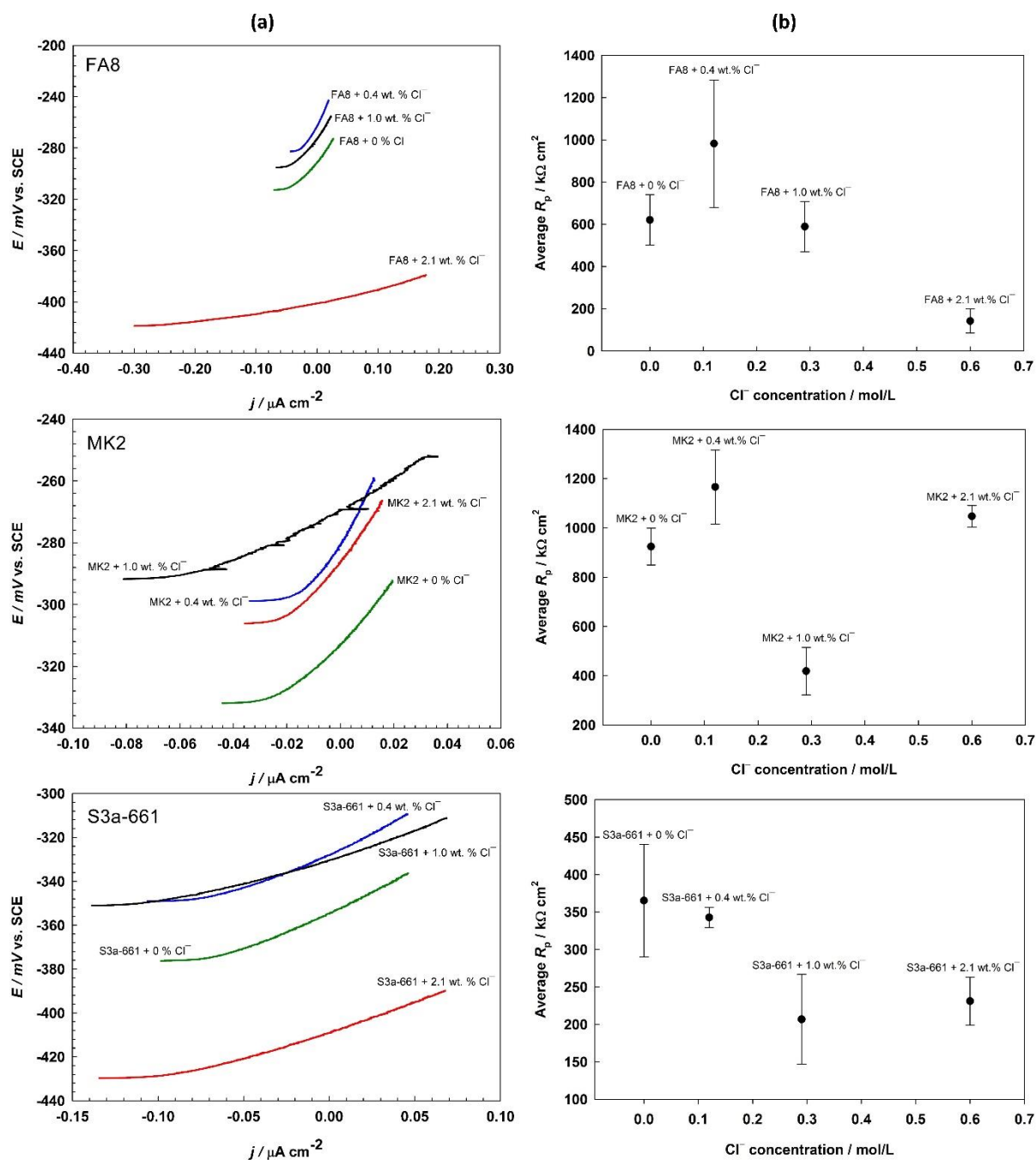


Figure 1. a) Representative LPR spectra and b) average polarization resistance (R_p) values measured in the three bare AAM pore solutions (Table 1) and in those with added Cl^- at concentrations of 0.4 %, 1.0 % and 2.1 %.

LPR measurements revealed quite different corrosion behaviour in the OPC pore solution (Figure 2, Supplement Figure 2). Polarisation resistance values (R_p) in the OPC pore solution without chlorides ($823 \text{ k}\Omega \text{ cm}^2$) are comparable to those measured in the MK2 pore solution ($924 \text{ k}\Omega \text{ cm}^2$), while in the other AAM pore solutions the values are lower. When Cl^- ions are added to OPC pore solution, the measured R_p values are significantly lower (dropping to below $10 \text{ k}\Omega \text{ cm}^2$). The exact Cl^- concentration does not seem to have much of an influence on the R_p values; LPR measurements in OPC pore solution showed similar R_p values at all three Cl^- concentrations: 0.4 % ($8 \text{ k}\Omega \text{ cm}^2$), 1.0 % ($5 \text{ k}\Omega \text{ cm}^2$) and 2.1 % ($6 \text{ k}\Omega \text{ cm}^2$) due to a loss of passivity.

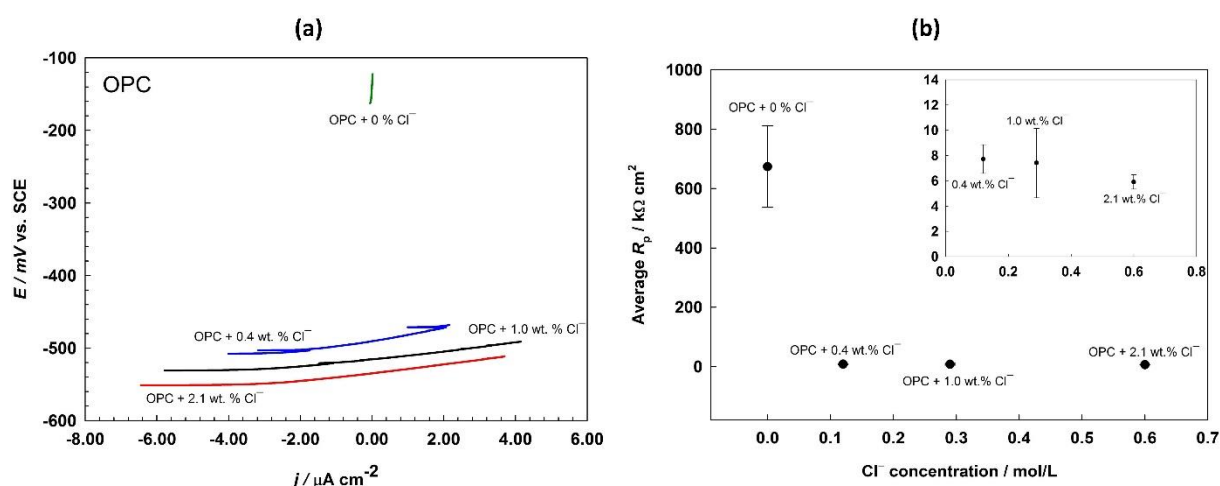


Figure 2. a) Representative LPR spectra and b) average polarization resistance (R_p) values measured in the bare OPC pore solution (0.031M NaOH) and the same solution with added Cl^- at various concentrations (0.4 %, 1.0 % and 2.1 %).

Figure 3 (and Supplement Figure 3) presents cyclic potentiodynamic polarisation (CPD) measurements carried out on steel in the different simulated AAM pore solutions. The purpose of the cyclic potentiodynamic polarization (CPD) scans was to determine the susceptibility of the steel to different types of corrosion i.e. general or local. As can be observed from the CPD curves in Figure 3, the shape of the curves is similar in all the pore solutions, both with and

without the addition of chlorides. CPD curves of the steel in the various pore solutions exhibit a pseudo passive region. When the potential is reversed, negative hysteresis can be observed, indicating that steel pitting is unlikely to occur in this environment. Current density (j_{corr}) values measured in the pore solutions without chlorides showed similarly low values, corresponding to corrosion rates of approximately 1 $\mu\text{m}/\text{year}$. When 1 % Cl^- was added to the pore solutions, the corrosion rates increased in all solutions, by between 40 to 90 %. Results from the CPD correspond well with those obtained using LPR techniques.

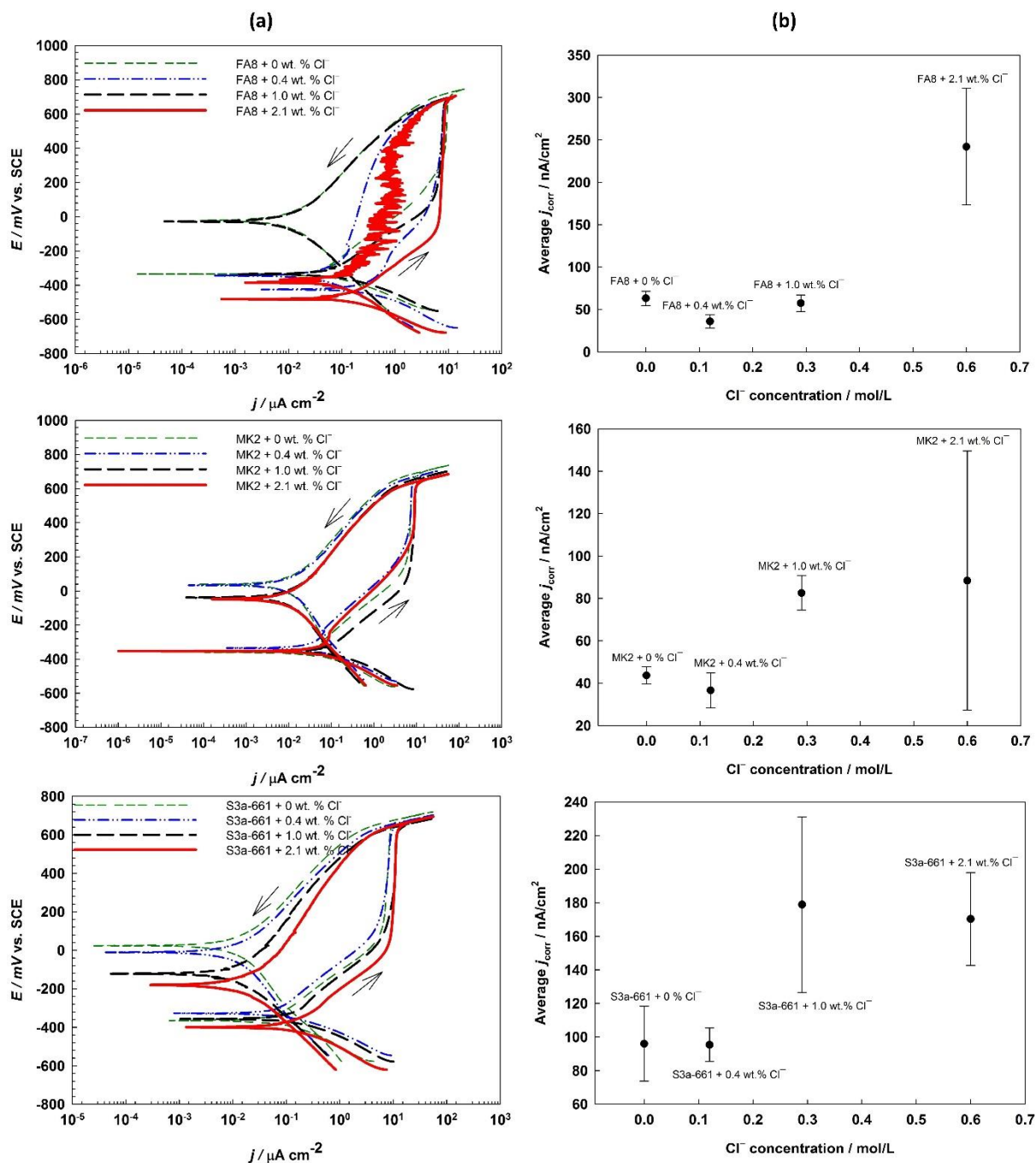


Figure 3. a) Representative CPD spectra and b) average current density (j_{corr}) values measured in the three bare AAM pore solutions (Table 1) and those with added Cl^- concentrations of 0.4 %, 1.0 % and 2.1 % .

Figure 4 (and Supplement Figure 4) shows that the CPD curves measured in the OPC pore solution (with and without Cl^-) significantly differ from those measured in the AAM pore

solutions (Figure 3). Unlike in the AAMs, negative hysteresis was only measured in the OPC pore solution when Cl^- had not been added. Positive hysteresis, which relates to a general type of corrosion, was observed even at the lowest Cl^- concentration (0.4 %), and remained positive at higher Cl^- concentrations. Unlike the results from the AAM pore solutions, this indicates that the steel is prone to pitting corrosion in OPC environments contaminated with chloride. Although corrosion current density (j_{corr}) values are somewhat comparable in the OPC ($0.037 \mu\text{A}/\text{cm}^2$) and AAM pore solutions (up to $0.096 \mu\text{A}/\text{cm}^2$), in OPC the j_{corr} increases significantly when Cl^- is added, with j_{corr} values ($3.01 \mu\text{A}/\text{cm}^2$) being one order magnitude higher than in the AAMs (up to $0.2 \mu\text{A}/\text{cm}^2$) when in the presence of chlorides.

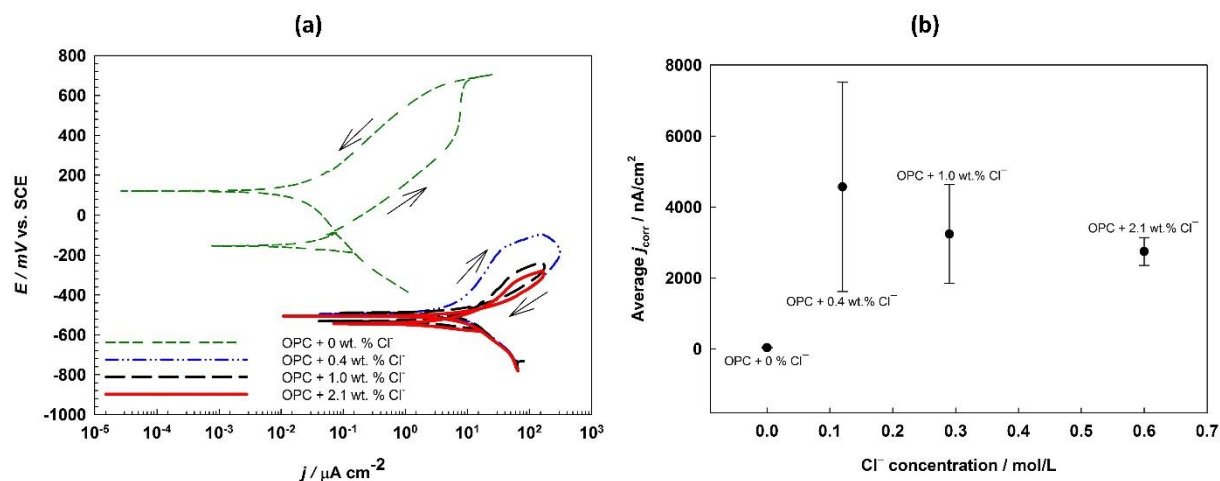


Figure 4. a) Representative CPD spectra and b) average current density (j_{corr}) values measured in the bare OPC pore solution (0.031M NaOH) and the same solution with added Cl^- at concentrations of 0.4 %, 1.0 % and 2.1 %.

Electrochemical impedance (EIS) was measured in both the simulated AAM pore solutions (Table 1) and the same solutions with the addition of Cl^- at concentrations of 0.4 %, 1.0 % and 2.1 %.

Impedance responses in all pore solutions, whether with or without the added chlorides, have a similar shape (presented as Nyquist and Bode plots in Figure 5, Supplement Figure 5). There

are small differences between the average impedance values measured in the various solutions (Figure 7). The total impedance ($|Z_{\text{total}}|$) values measured in solutions without added chlorides are relatively high, representing average corrosion rates of less than 1 $\mu\text{m}/\text{year}$. No significant decrease in the $|Z_{\text{total}}|$ values (and consequently no increase in the corrosion rates) was observed in the MK2 and S3a-661 pore solutions with added chlorides (approximately 1.5 \times), while the corrosion rate in the FA8 pore solution was 3.2 \times higher when 2.1 % Cl^- was added.

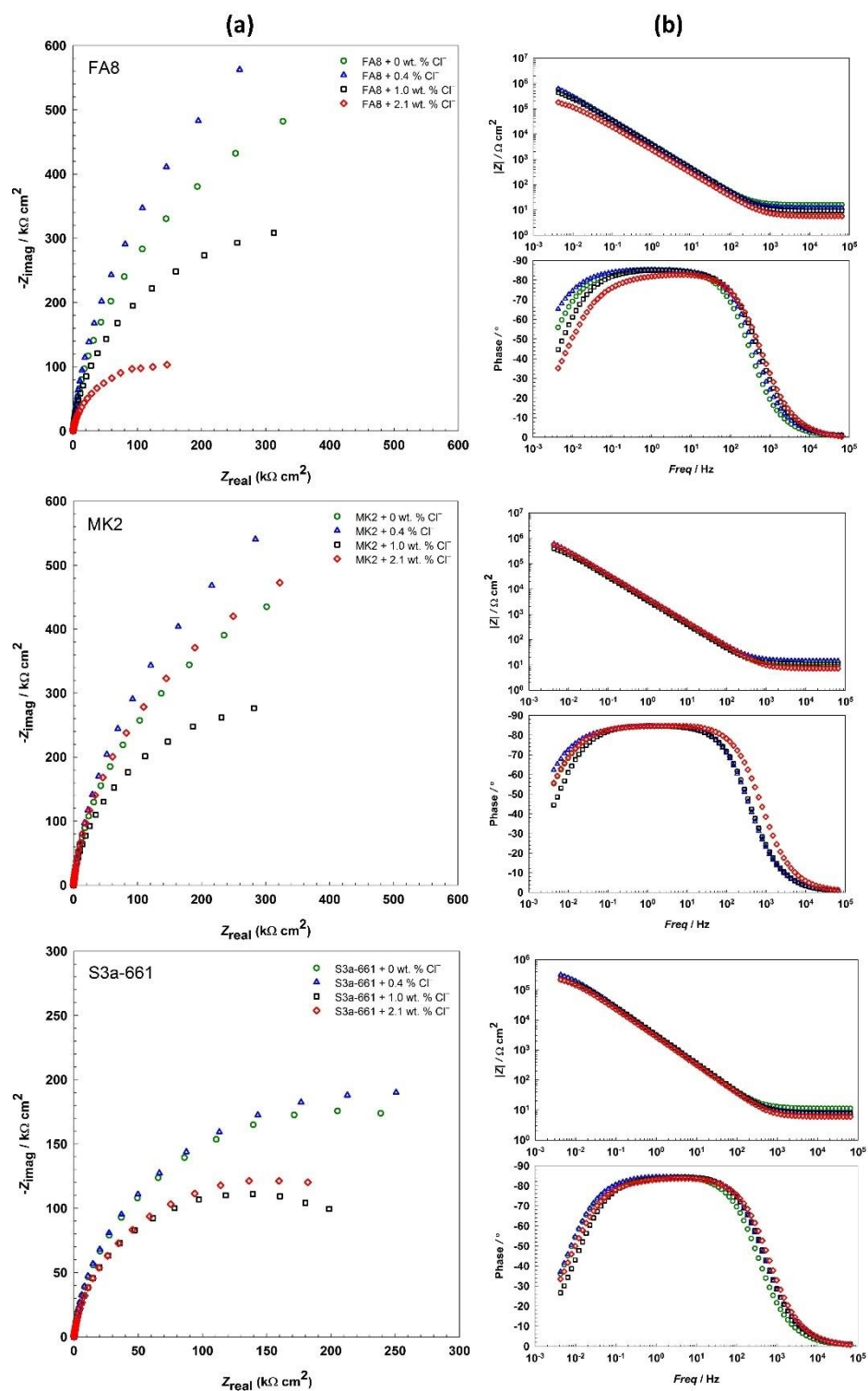


Figure 5. a) Nyquist EIS spectra and b) representative Bode EIS spectra measured in the three bare AAM pore solutions (Table 1) and those with added Cl^- at concentrations of 0.4 %, 1.0 % and 2.1 %.

The shape of the impedance spectrum in the OPC pore solution (Figure 6) without Cl^- is similar to that observed in the AAM pore solutions (Figure 5). The total impedance ($|Z_{\text{total}}|$) value measured in the OPC without added chlorides is also relatively high ($401 \text{ k}\Omega \text{ cm}^2$), representing an average corrosion rate below $1 \mu\text{m}/\text{year}$. After adding chlorides to the OPC pore solution, the impedance spectra changed substantially, affecting the impedance magnitude and phase shifts, and thus indicating the occurrence of a change in electrochemical processes. Unlike in the AAM pore solutions, $|Z_{\text{total}}|$ values decrease significantly when Cl^- are added to the OPC pore solution ($\sim 4 \text{ k}\Omega \text{ cm}^2$) and showing that there is no important difference between the different concentrations of Cl^- (Figure 6, Figure 7).

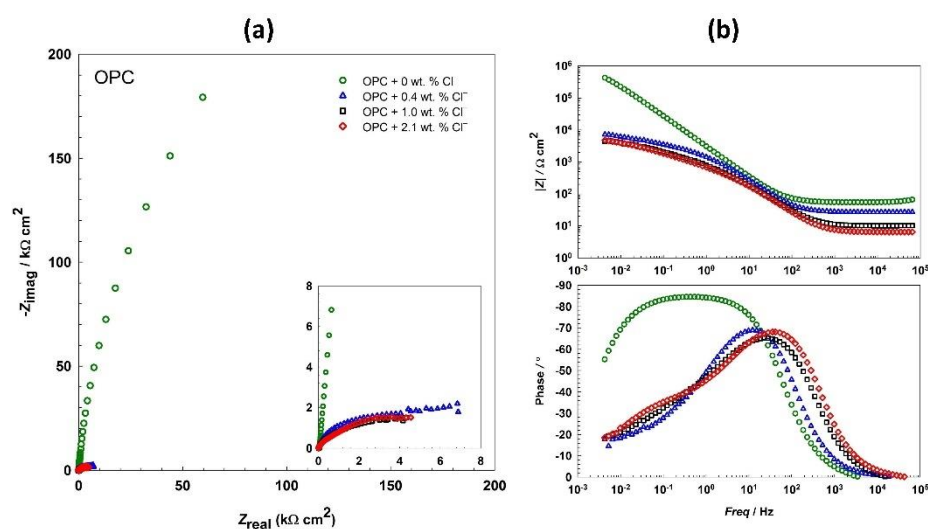


Figure 6. a) Nyquist EIS spectra and b) representative Bode EIS spectra measured in the bare OPC pore solution (0.031M NaOH) and the same solution with added Cl^- at concentrations of 0.4 %, 1.0 % and 2.1 %.

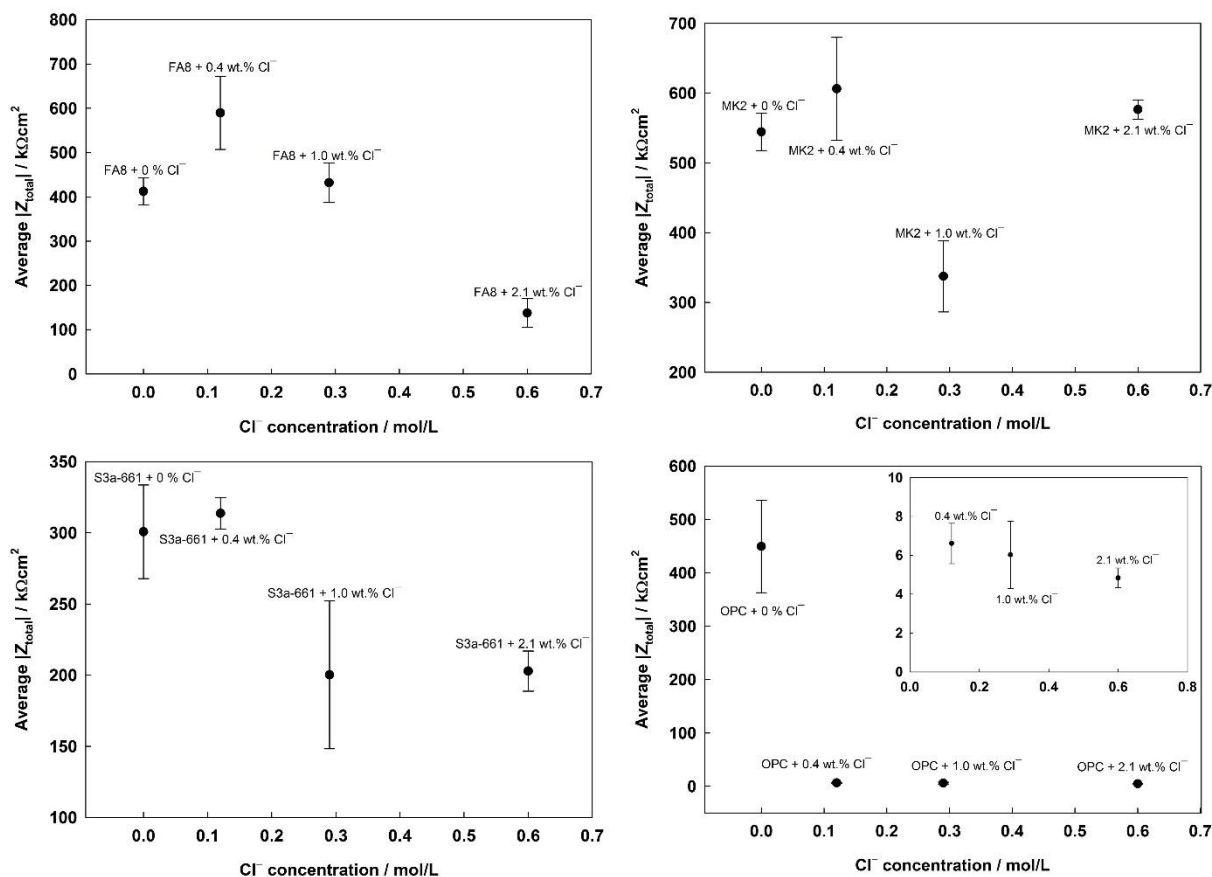


Figure 7. Average total impedance ($|Z_{total}|$) values at the lowest measured frequency in the three AAM pore solutions (Table 1), the OPC pore solution (0.031M NaOH), and the same solutions with the addition of Cl^- to concentrations of either 0.4 %, 1.0 % and 2.1 %.

In the present corrosion study of steel in simulated pore solutions, various parameters, including polarisation resistance (LPR) measurements, electrical impedance spectroscopy (EIS) and cyclic potentiodynamic polarization (CPD) scans, were measured and then used to calculate corrosion rates. The Stern-Geary equation (Equation 1) was used to calculate j_{corr} values, while v_{corr} values were calculated according to Equation 2, as described in the chapter ‘Materials and Methods’. There is good agreement across all the electrochemical methods (Table 3) with respect to each individual pore solution. Comparing the various AAM pore solutions, the highest corrosion rate was measured in FA8 with 2.1 % Cl^- , where it was 2.8 $\mu m/year$. It can also be concluded that the corrosion resistance of steel only reduced slightly when a certain

chloride concentration was reached; this occurred at 2.1 % Cl^- in FA8 and 1 % Cl^- in S3a-661, while in MK2 the corrosion resistance did not change significantly, even at a concentration of 2.1 % Cl^- .

The v_{corr} values measured in the bare OPC pore solution (without the addition of Cl^-) are fairly comparable with those measured in the AAM pore solutions (Table 3). On the contrary, however, the maximum increase in v_{corr} in the OPC solution with the addition of Cl^- was almost 130 times higher than the original (bare) OPC solution, compared to a Cl^- -induced difference was only 5 times higher in the AAM solutions.

Table 3. Average corrosion rate (v_{corr}) values of steel in the various pore solutions (Table 1), both with and without the addition of Cl^- (to concentrations of 0.4 %, 1.0 % and 2.1 %), as calculated from parameters measured using three electrochemical techniques (LPR, CPD and EIS).

Method		LPR	CPD	EIS	
Pore solution type		v_{corr} [$\mu\text{m}/\text{year}$]	v_{corr} [$\mu\text{m}/\text{year}$]	v_{corr} [$\mu\text{m}/\text{year}$]	
0 (wt.) % Cl^-	AAM	FA8	0.5 ± 0.1	0.7 ± 0.1	0.7 ± 0.1
		MK2	0.3 ± 0.0	0.5 ± 0.1	0.6 ± 0.0
		S3a-661	0.9 ± 0.2	1.1 ± 0.3	1.0 ± 0.1
	OPC	0.031M NaOH	0.4 ± 0.1	0.4 ± 0.1	0.7 ± 0.1
0.4 (wt.) % Cl^-	AAM	FA8	0.3 ± 0.1	0.4 ± 0.1	0.5 ± 0.1
		MK2	0.3 ± 0.0	0.4 ± 0.1	0.5 ± 0.1
		S3a-661	0.9 ± 0.0	1.1 ± 0.1	1.0 ± 0.0
	OPC	0.031M NaOH	40 ± 5.9	53 ± 34	47 ± 8.0
1.0 (wt.) % Cl^-	AAM	FA8	0.5 ± 0.1	0.7 ± 0.1	0.7 ± 0.1
		MK2	0.8 ± 0.2	1.0 ± 0.1	0.9 ± 0.2
		S3a-661	1.6 ± 0.4	2.1 ± 0.7	1.6 ± 0.5
	OPC	0.031M NaOH	45 ± 14	38 ± 16	53 ± 15
2.1 (wt.) % Cl^-	AAM	FA8	2.5 ± 1.1	2.8 ± 1.1	2.3 ± 0.7
		MK2	0.3 ± 0.0	1.0 ± 0.8	0.5 ± 0.0
		S3a-661	1.3 ± 0.2	2.0 ± 0.4	1.5 ± 0.1
	OPC	0.031M NaOH	51 ± 4.8	32 ± 4.6	63 ± 6.6

There are advantages and limitations of each individual electrochemical technique. Electrochemical impedance spectroscopy (EIS) and linear polarisation resistance (LPR)

measurements do not affect the kinetics of natural corrosion processes and enable relatively good correlation between the R_p values measured and corrosion rate (v_{corr}) calculated. Cyclic potentiodynamic polarization (CPD), on the other hand, interferes with natural corrosion processes with externally applied potential, meaning quantitative correlation between the parameters measured and the corrosion rate is not accurate. CPD curves can, however, provide qualitative information regarding the passivity of the steel and its susceptibility to pitting corrosion in selected environments.

In order to further study the susceptibility of steel corrosion in pore solutions, steel electrodes were scratched and then immersed in all the pore solutions used in this study i.e. the three bare AAM pore solutions, the OPC pore solution, and each of these with and without the addition of varying amounts of Cl^- (to concentrations of 0.4 %, 1.0 %, 2.1 %). After 27 days of exposure the electrodes were visually analysed and compared (Figure 8). Visual analysis of the extent and type of corrosion damage confirmed the results obtained from electrochemical techniques. Electrodes exposed to the AAM pore solution showed very little corrosion damage on the surface of the exposed steel, even when solutions contained the highest concentration of Cl^- (2.1 %). On the contrary, local corrosion damage occurred on the ordinary OPC solutions and it was far more severe.

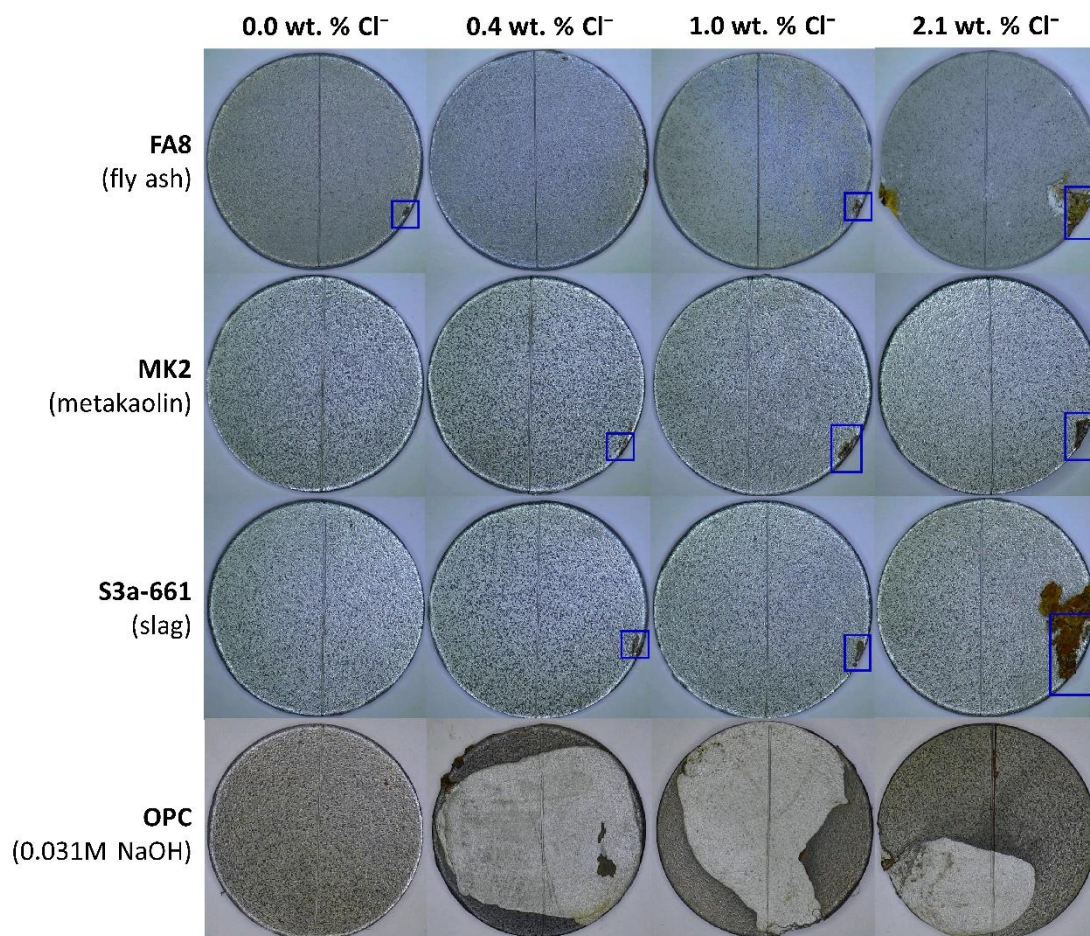


Figure 8. Visual analysis of the steel samples exposed to the three AAM pore solutions and the OPC pore solution (Table 1), both with and without the addition of Cl^- in various concentrations (0.4 %, 1.0 % and 2.1 %); \square the blue rectangles indicate crevice corrosion at the point where the steel samples made contact with the Teflon holder.

Following the addition of Cl^- ions, diverse responses were observed in the various pore solutions.

The results clearly show that the processes of steel corrosion were substantially different in the simulated AAMs pore solutions than in the simulated OPC pore solutions. All electrochemical techniques measured small corrosion rates in the AAM pore solutions, even when the Cl^- concentrations were high. Minor differences were shown between the corrosion rates measured in the various AAM solutions. Furthermore, this observation was in complete agreement with

the surface analysis, which showed no corrosion damage or corrosion products at the surface of the exposed specimen (Figure 8).

The corrosion rates of steel in OPC simulated pore solutions are generally lower than that of steel embedded in OPC mortars [21]. Comparisons of studies in mortars and in their pore solutions show that measured corrosion rate values in pore solution can go up to a couple of hundreds $\mu\text{m}/\text{year}$ [22], while the (local) corrosion rates in solid mortars can be 10-times higher [23]. According to one of our previous studies investigating solid AAM mortars [16], a similar relationship was expected between the corrosion rates in the AAMs. In line with OPC, it was foreseen that more general corrosion damage, and somewhat lower corrosion rates, would be detected in the simulated AAM pore solutions compared to those in the AAM mortar specimens. Surprisingly, the differences observed were not only minor, but in fact no corrosion damage was found, with the corrosion rates measured in the AAM pore solutions being insignificant. According to the authors' knowledge, such a discrepancy has not previously been reported in the scientific literature.

Several reasons can be assumed for the near passive state of steel in the AAM pore solutions. In solid porous materials (including both OCP mortars and AAMs), the dynamics of corrosion processes are different to in solutions; the corrosion kinetics are different for steel embedded in concrete compared to steel in a solution, despite the fact that the thermodynamic situation is similar [24,25]. Porosity affects transport of the electrolytes and oxygen, and causes spatial separation between the anodic and cathodic sites [9,10]. By itself, this does not explain the huge difference between the corrosion rates in the AAM and OCP solutions, but it is supposed that the cathodic reactions in the AAMs are more strongly dependent on the oxygen content than in OPC. Conversely, this could be due to the higher concentration of sulphate ions in the AAM pore solutions (Table 1). The inhibiting effect of sulphate ions has been reported previously [26]. Namely, sulphate ions in environments containing chloride have an inhibitive

effect on pitting corrosion in reinforcing steel [27]. A similar effect has been observed on ferritic stainless steel, where the presence of sulphate ions together with chlorides shifted the pitting potential to more positive values [28]. It has also been reported that meta-silicate ions (SiO_3^{2-}) can protect the surface of austenitic stainless steel from chloride ions, by adsorbing and suppressing metal dissolution and pit growth [29].

Unlike the AAM solutions, the generic OPC pore solution used in this study does not contain any sulphate or meta-silicate ions (Table 1). In this study a generic OPC pore solution (0.031M NaOH) was used. In our previous study [22] pore solutions were extracted from mortar mixes made of different types of cement. A comparison of results from the two studies, obtained from both real and generic OPC pore solutions, confirm that the CPD spectra exhibit a similar shape, and that the corrosion rates measured are of the same order of magnitude.

Table 4. $\frac{[\text{Cl}^-]}{[\text{SO}_4^{2-}]}$ ratios in the pore solutions, taking into account both the existing (Table 1) and added Cl^- concentrations.

Pore solutions	PH	Added Cl^- concentrations			
		0.0 wt. % Cl^-	0.4 wt. % Cl^-	1.0 wt. % Cl^-	2.1 wt. % Cl^-
FA8	12.4	0.0053	0.712	1.715	3.54
MK2	12.5	0.377	49.3	118	245
S3a-661	12.7	1.023	23.9	56.3	115
OPC	12.8	-	-	-	-

It can be deduced from Table 4, and the results presented in Figure 1, Figure 3 and Figure 5, that in the fly ash mortar pore solution (FA8), which contains a high concentration of sulphate ions, reduced passivity is observed only when the $[\text{Cl}^-]/[\text{SO}_4^{2-}]$ ratio is ≥ 1.715 . In the metakaolin (MK2) and slag (S3a-661) pore solutions, the smaller increase in Cl^- ions (0.4 wt. %) does not appear to have a drastic effect, since the R_p values do not decrease to a great extent. In this case the $\text{Si}_2\text{O}_5^{2-}$ ions probably also play a role, where their concentration is higher than in the case of FA8 (see Table 1).

4 CONCLUSIONS

This paper presents a corrosion study of steel exposed to pore solutions extracted from alkali-activated mortars based on either fly ash (FA8), metakaolin (MK2) or slag (S3a-661). A generic ordinary Portland cement pore solution (OPC) was also used for purposes of comparison. The following conclusions can be drawn:

- Very low steel corrosion rates were measured in the simulated AAMs solutions using all electrochemical methods, regardless of the Cl^- content. These results were in agreement with the surface analysis, which showed no evidence of corrosion damage or the presence of corrosion products.
- All electrochemical methods detected a strong shift in the corrosion rates of steel in the simulated OPC solutions when the Cl^- content was increased. These results were in agreement with the surface analysis, which showed evidence of corrosion damage and the presence of corrosion products.
- A huge discrepancy was found between the corrosion processes on steel embedded in the AAM mortars and that in the AAM simulated pore solutions, which was not the case for OPC.
- A few potential explanations were proposed for the discrepancy between the corrosion processes existing on steel embedded in the AAM mortars compared to those in the simulated AAM pore solutions, but none of them could explain the nearly passive state of steel in the AAM solutions. Further comprehensive studies are therefore needed to explain this passivity, as well as to determine the crucial parameters that control corrosion processes in specific AAMs.

ACKNOWLEDGEMENTS

The work described in this paper forms parts of the bilateral research project “Phenomenological modelling of steel corrosion in concretes for service life prediction”, which was financed by the Slovenian Research Agency (ARRS) and the French Alternative Energies and Atomic Energy Commission (CEA). The financial support received from the Slovenian Research Agency (ARRS) through the research programme P2-0273 “Building structures and materials” is gratefully acknowledged. The authors would like to thank Dr. Valérie L'Hostis and the team from Service d'Etude du Comportement des Radionucléides, CEA, Université Paris-Saclay, for providing equipment and their professional help in extracting and analysing the pore solutions used in this research. The authors would also like to thank Dr. Vilma Ducman and her team from the Laboratory for Cements, Mortars and Ceramics, ZAG, for their help with the selection and preparation of alkali-activated mortars.

AUTHOR CONTRIBUTIONS

N.G. was involved in the conceptualization of the study, investigation, formal analysis, and writing the original draft of the manuscript. T.K. was involved in the conceptualization, formal analysis, writing (through reviewing and editing), and supervision. S.P. was involved in supervising the study and acquiring funding. A.L. was involved in the writing (through reviewing and editing), supervising the study and acquiring funding.

CONFLICT OF INTEREST

The authors declare no financial or commercial conflict of interest.

DATA AVAILABILITY STATEMENT

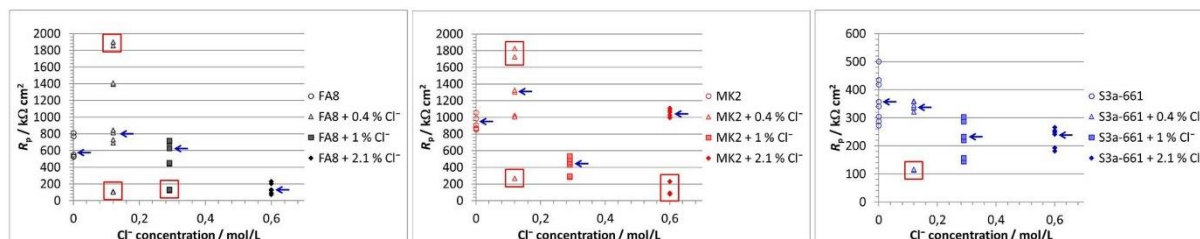
The data that supports the findings of this study are available from the corresponding author upon reasonable request.

REFERENCES

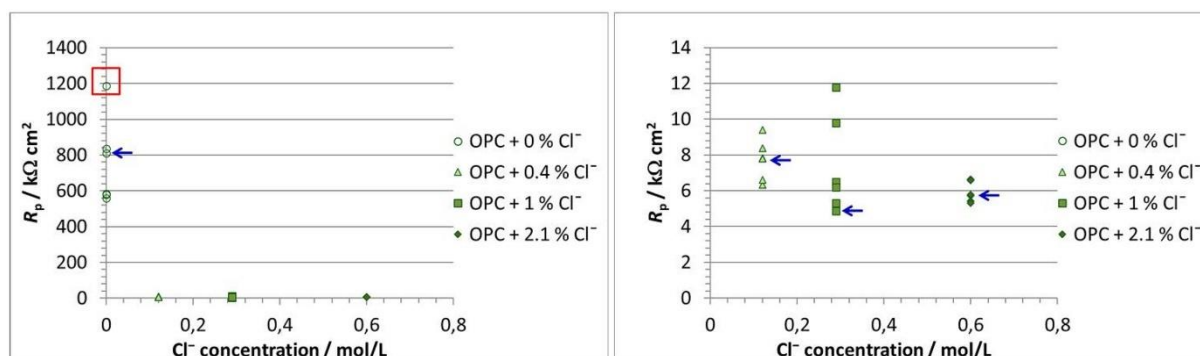
1. Scrivener, K.L.; Kirkpatrick, R.J. Innovation in Use and Research on Cementitious Material. *Cement and Concrete Research* **2008**, *38*, 128–136, doi:10.1016/j.cemconres.2007.09.025.
2. Van Deventer, J.S.J. Chapter 10 - Progress in the Adoption of Geopolymer Cement. In *Handbook of Low Carbon Concrete*; Nazari, A., Sanjayan, J.G., Eds.; Butterworth-Heinemann: Oxford, UK, 2017; pp. 217–262 ISBN 978-0-12-804524-4.
3. Provis, J.L.; Bernal, S.A. Geopolymers and Related Alkali-Activated Materials. *Annu. Rev. Mater. Res.* **2014**, *44*, 299–327, doi:10.1146/annurev-matsci-070813-113515.
4. Provis, J.L. Alkali-Activated Materials. *Cement and Concrete Research* **2018**, *114*, 40–48, doi:10.1016/j.cemconres.2017.02.009.
5. Shi, C.; Roy, D.; Krivenko, P. *Alkali-Activated Cements and Concretes*; CRC Press, Taylor & Francis: London, UK, 2006; ISBN 978-0-415-70004-7.
6. Kong, D.L.Y.; Sanjayan, J.G. Effect of Elevated Temperatures on Geopolymer Paste, Mortar and Concrete. *Cement and Concrete Research* **2010**, *40*, 334–339, doi:10.1016/j.cemconres.2009.10.017.
7. Bakri, A.M.M.A.; Kamarudin, H.; Binhussain, M.; Nizar, I.K.; Rafiza, A.R.; Zarina, Y. Comparison of Geopolymer Fly Ash and Ordinary Portland Cement to the Strength of Concrete. *Advanced Science Letters* **2013**, *19*, 3592–3595, doi:10.1166/asl.2013.5187.
8. Ofer-Rozovsky, E.; Haddad, M.A.; Bar-Nes, G.; Borojovich, E.J.C.; Binyamini, A.; Nikolski, A.; Katz, A. Cesium Immobilization in Nitrate-Bearing Metakaolin-Based Geopolymers. *Journal of Nuclear Materials* **2019**, *514*, 247–254, doi:10.1016/j.jnucmat.2018.11.003.
9. Alonso, C.; Andrade, C.; González, J.A. Relation between Resistivity and Corrosion Rate of Reinforcements in Carbonated Mortar Made with Several Cement Types. *Cement and Concrete Research* **1988**, *18*, 687–698, doi:10.1016/0008-8846(88)90091-9.
10. Glass, G.K.; Page, C.L.; Short, N.R. Factors Affecting the Corrosion Rate of Steel in Carbonated Mortars. *Corrosion Science* **1991**, *32*, 1283–1294, doi:10.1016/0010-938X(91)90048-T.
11. Criado, M.; Provis, J.L. Alkali Activated Slag Mortars Provide High Resistance to Chloride-Induced Corrosion of Steel. *Front. Mater.* **2018**, *5*, doi:10.3389/fmats.2018.00034.
12. Provis, J.L.; Arbi, K.; Bernal, S.A.; Bondar, D.; Buchwald, A.; Castel, A.; Chithiraputhiran, S.; Cyr, M.; Dehghan, A.; Dombrowski-Daube, K.; et al. RILEM TC 247-DTA Round Robin Test: Mix Design and Reproducibility of Compressive Strength of Alkali-Activated Concretes. *Mater Struct* **2019**, *52*, 99, doi:10.1617/s11527-019-1396-z.
13. Gluth, G.J.G.; Arbi, K.; Bernal, S.A.; Bondar, D.; Castel, A.; Chithiraputhiran, S.; Dehghan, A.; Dombrowski-Daube, K.; Dubey, A.; Ducman, V.; et al. RILEM TC 247-DTA Round Robin Test: Carbonation and Chloride Penetration Testing of Alkali-Activated Concretes. *Mater Struct* **2020**, *53*, 21, doi:10.1617/s11527-020-1449-3.
14. Winnefeld, F.; Gluth, G.J.G.; Bernal, S.A.; Bignozzi, M.C.; Carabba, L.; Chithiraputhiran, S.; Dehghan, A.; Dolenc, S.; Dombrowski-Daube, K.; Dubey, A.; et al. RILEM TC 247-DTA Round Robin Test: Sulfate Resistance, Alkali-Silica Reaction and Freeze–Thaw Resistance of Alkali-Activated Concretes. *Mater Struct* **2020**, *53*, 140, doi:10.1617/s11527-020-01562-0.
15. Gluth, G.; Rickard, W. Design and Characterization of Fly Ash-Based Geopolymer Concretes for a Round-Robin Durability Testing Program. In *Proceedings of the Geopolymers: the route to eliminate waste and emissions in ceramic and cement*

- manufacturing; Leonelli, C., Romagnoli, M., Eds.; Engineering Conferences International / Società Ceramica Italiana: Hernstein, Austria, 2015; pp. 67–70.
16. Gartner, N.; Hren, M.; Kosec, T.; Legat, A. Characterizing Steel Corrosion in Different Alkali-Activated Mortars. *Materials* **2021**, *14*, 7366, doi:10.3390/ma14237366.
 17. Cyr, M.; Daidié, A. Optimization of a High-Pressure Pore Water Extraction Device. *Review of Scientific Instruments* **2007**, *78*, 023906, doi:10.1063/1.2428273.
 18. Cyr, M.; Rivard, P.; Labrecque, F.; Daidié, A. High-Pressure Device for Fluid Extraction from Porous Materials: Application to Cement-Based Materials. *Journal of the American Ceramic Society* **2008**, *91*, 2653–2658, doi:10.1111/j.1551-2916.2008.02525.x.
 19. Schiegg, Y. Monitoring of Corrosion in Reinforced Concrete Structures. In *Corrosion in Reinforced Concrete Structures*; Böhni, H., Ed.; Woodhead Publishing Limited: Cambridge, England, 2005; pp. 46–70 ISBN 978-1-84569-043-4.
 20. Kelly, R.G.; Scully, J.R.; Shoosmith, D.W.; Buchheit, R.G. *Electrochemical Techniques in Corrosion Science and Engineering*; Marcel Dekker, Inc.: New York, NY, USA, 2003; ISBN 0-8247-9917-8.
 21. Legat, A.; Leban, M.; Bajt, Ž. Corrosion Processes of Steel in Concrete Characterized by Means of Electrochemical Noise. *Electrochimica Acta* **2004**, *49*, 2741–2751, doi:10.1016/j.electacta.2004.01.036.
 22. Hren, M.; Kosec, T.; Legat, A. Corrosion Behavior of Steel in Pore Solutions Extracted from Different Blended Cements. *Materials and Corrosion* **2020**, *71*, 759–766, doi:10.1002/maco.202011548.
 23. Hren, M.; Bokan Bosiljkov, V.; Legat, A. Effects of Blended Cements and Carbonation on Chloride-Induced Corrosion Propagation. *Cement and Concrete Research* **2021**, *145*, 106458, doi:10.1016/j.cemconres.2021.106458.
 24. Gonzalez, J.A.; Algaba, J.S.; Andrade, C. Corrosion of Reinforcing Bars in Carbonated Concrete. *British Corrosion Journal* **1980**, *15*, 135–139, doi:10.1179/bcj.1980.15.3.135.
 25. Angst, U.; Elsener, B.; Larsen, C.K.; Vennesland, Ø. Chloride Induced Reinforcement Corrosion: Rate Limiting Step of Early Pitting Corrosion. *Electrochimica Acta* **2011**, *56*, 5877–5889, doi:10.1016/j.electacta.2011.04.124.
 26. Huet, B.; L’Hostis, V.; Tricheux, L.; Idrissi, H. Influence of Alkali, Silicate, and Sulfate Content of Carbonated Concrete Pore Solution on Mild Steel Corrosion Behavior. *Materials and Corrosion* **2010**, *61*, 111–124, doi:10.1002/maco.200905244.
 27. Chen, C.; Jiang, L.; Guo, M.-Z.; Xu, P.; Chen, L.; Zha, J. Effect of Sulfate Ions on Corrosion of Reinforced Steel Treated by DNA Corrosion Inhibitor in Simulated Concrete Pore Solution. *Construction and Building Materials* **2019**, *228*, 116752, doi:10.1016/j.conbuildmat.2019.116752.
 28. Sherbakov, A.I.; Dorofeeva, V.N.; Korosteleva, I.G.; Kasatkina, I.V.; Kornienko, L.P.; Kasatkin, V.E. Inhibition of Pitting Corrosion of AISI 420 (40X13) Stainless Steel in Low-Mineralized Water by Sulphate Ions. *International Journal of Corrosion and Scale Inhibition* **2020**, *9*, 519–525, doi:10.17675/2305-6894-2020-9-2-7.
 29. Munis, A.; Zheng, M.; Zhao, T. Effect of Sulfate and Meta-Silicate Ions on Pitting Corrosion of Stainless Steel-316 in Chloride Containing Simulated Coal Gasifier Aqueous Effluents. *Mater. Res. Express* **2019**, *6*, 076541, doi:10.1088/2053-1591/ab160e.

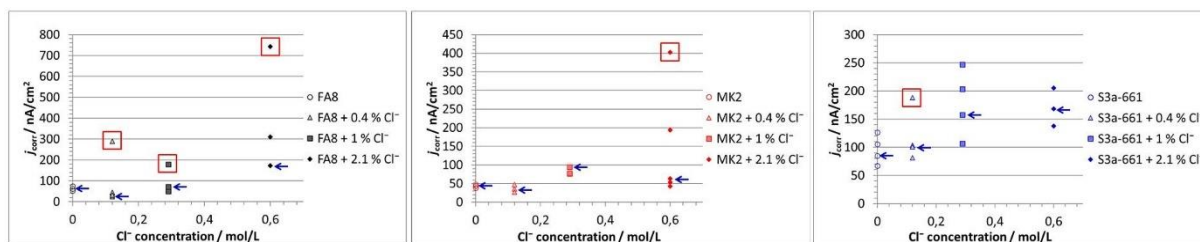
SUPPORTING INFORMATION



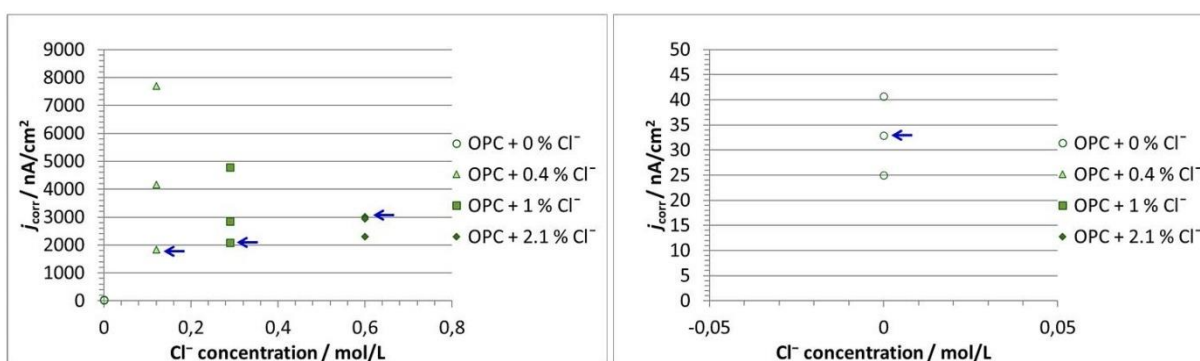
Supplement Figure 1. Scatter plot of the polarization resistance (R_p) values recorded in the three bare AAM pore solutions (Table 1) and those with added Cl^- at concentrations of 0.4 %, 1.0 % and 2.1 %. \square red rectangle represents the outliers; \rightarrow blue arrows show representative results are shown in Figure 1.



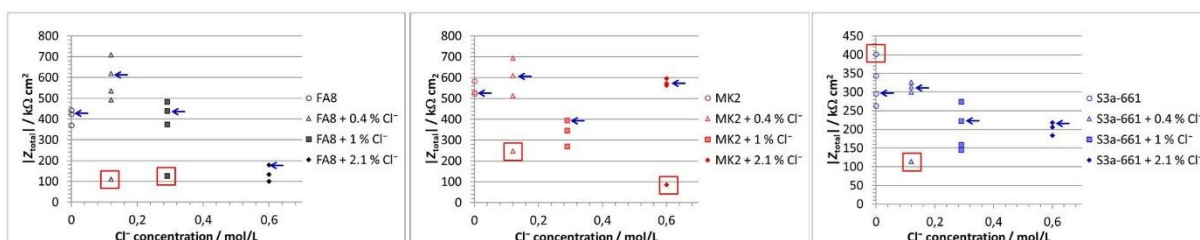
Supplement Figure 2. Scatter plot of the polarization resistance (R_p) values recorded in the three bare OPC pore solutions (Table 1) and those with added Cl^- at concentrations of 0.4 %, 1.0 % and 2.1 %. \square red rectangle represents the outliers; \rightarrow blue arrows show representative results are shown in Figure 2.



Supplement Figure 3. Scatter plot of current density (j_{corr}) values recorded in the three bare AAM pore solutions (Table 1) and those with added Cl^- at concentrations of 0.4 %, 1.0 % and 2.1 %. \square represents the outliers; \rightarrow representative results are shown in Figure 3.

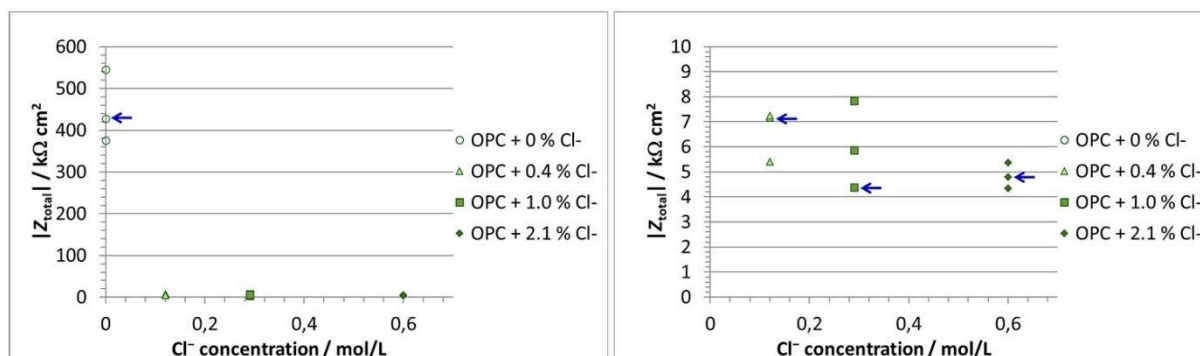


Supplement Figure 4. Scatter plot of current density (j_{corr}) values recorded in the three bare OPC pore solutions (Table 1) and those with added Cl^- at concentrations of 0.4 %, 1.0 % and 2.1 %. \square red rectangle represents the outliers; \rightarrow blue arrows show representative results are shown in Figure 4.



Supplement Figure 5. Scatter plot of total impedance ($|Z_{\text{total}}|$) values at the lowest measured frequency recorded in the three bare AAM pore solutions (Table 1) and those with added Cl^-

at concentrations of 0.4 %, 1.0 % and 2.1 %. \square red rectangle represents the outliers; \rightarrow blue arrows show representative results are shown in Figure 5.



Supplement Figure 6. Scatter plot of total impedance ($|Z_{\text{total}}|$) values at the lowest measured frequency recorded in the three bare OPC pore solutions (Table 1) and those with added Cl^- at concentrations of 0.4 %, 1.0 % and 2.1 %. \square red rectangle represents the outliers; \rightarrow blue arrows show representative results are shown in Figure 6.

FIGURES

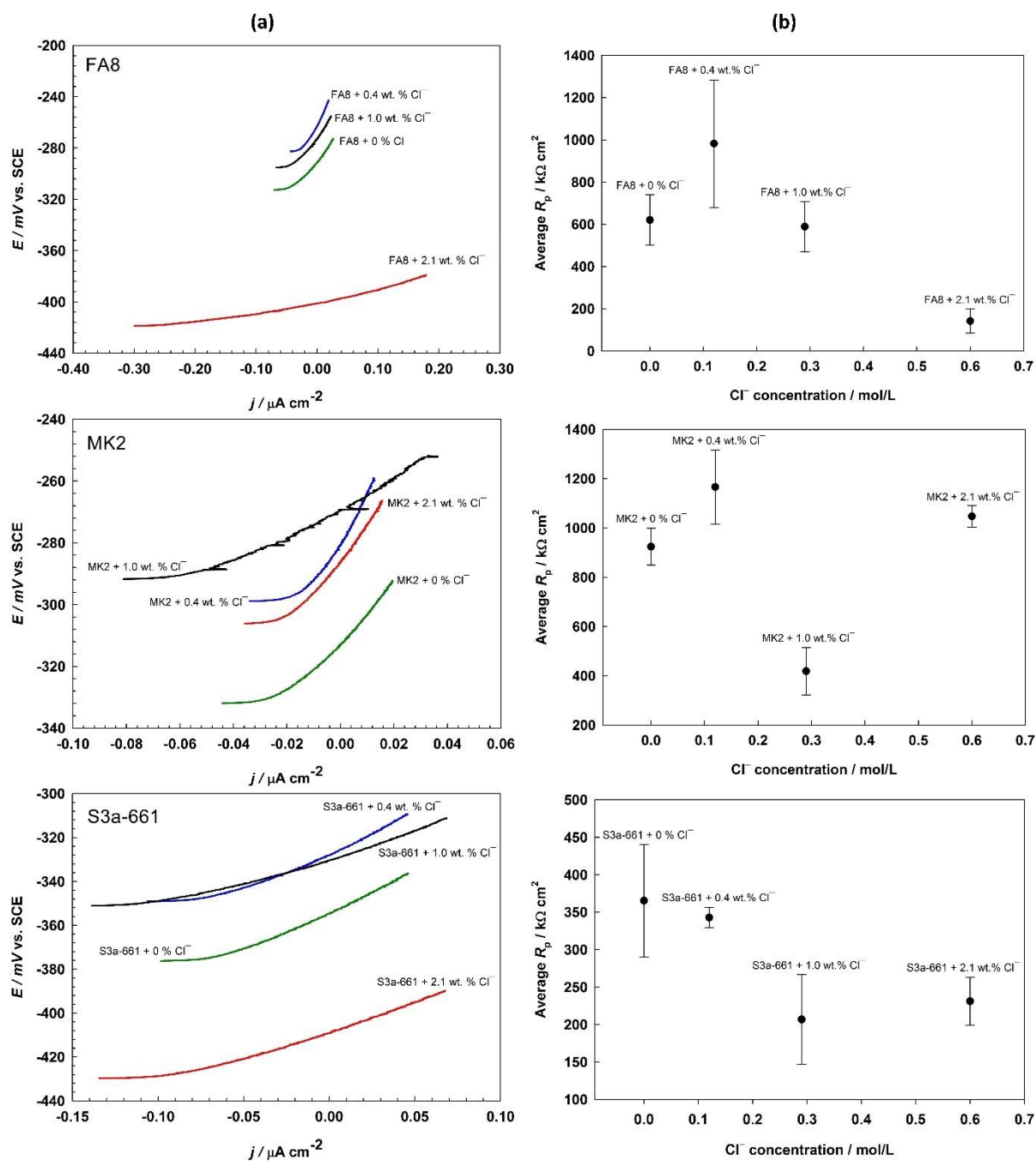


Figure 1. a) Representative LPR spectra and b) average polarization resistance (R_p) values measured in the three bare AAM pore solutions (Table 1) and in those with added Cl^- at concentrations of 0.4 %, 1.0 % and 2.1 %.

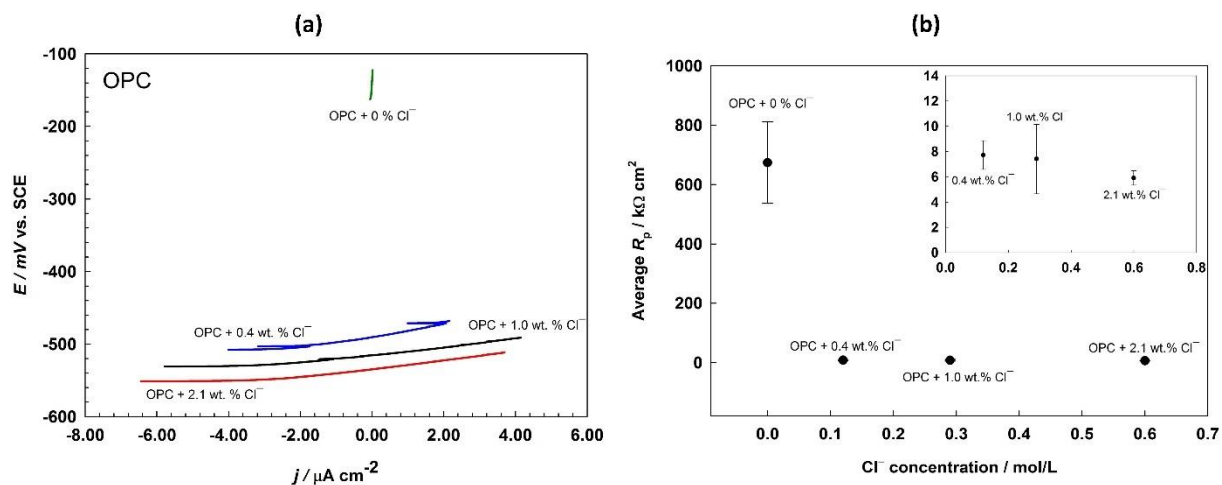


Figure 2. a) Representative LPR spectra and b) average polarization resistance (R_p) values measured in the bare OPC pore solution (0.031M NaOH) and the same solution with added Cl⁻ at various concentrations (0.4 %, 1.0 % and 2.1 %).

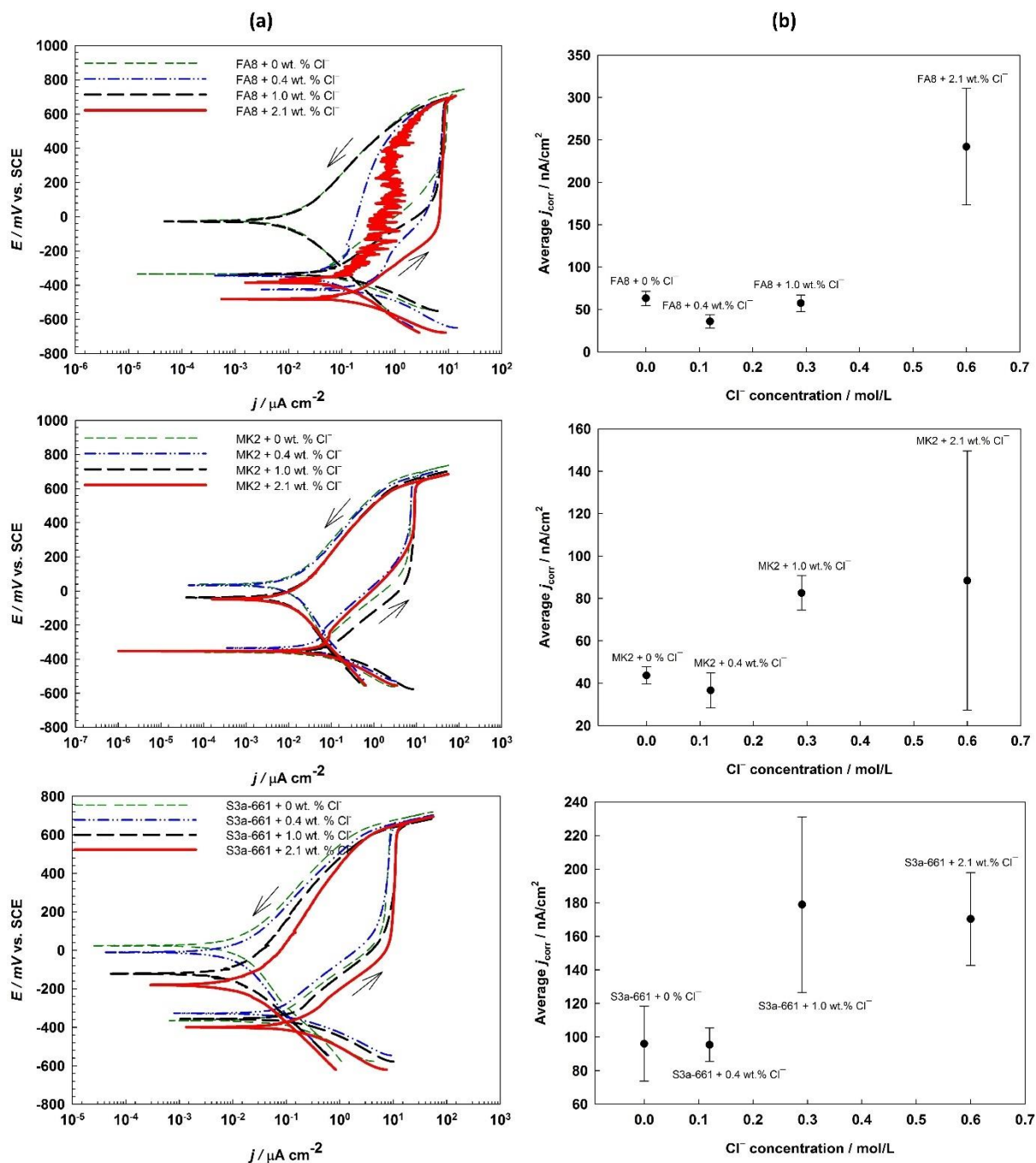


Figure 3. a) Representative CPD spectra and b) average current density (j_{corr}) values measured in the three bare AAM pore solutions (Table 1) and those with added Cl^- at concentrations of 0.4 %, 1.0 % and 2.1 % .

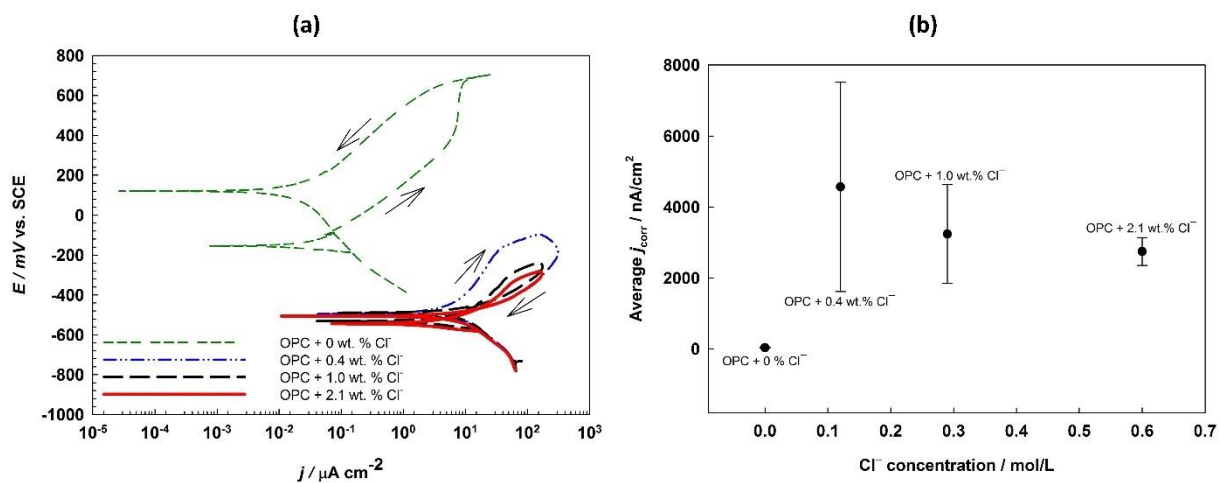


Figure 4. a) Representative CPD spectra and b) average current density (j_{corr}) values measured in the bare OPC pore solution (0.031M NaOH) and the same solution with added Cl^- at concentrations of 0.4 %, 1.0 % and 2.1 %.

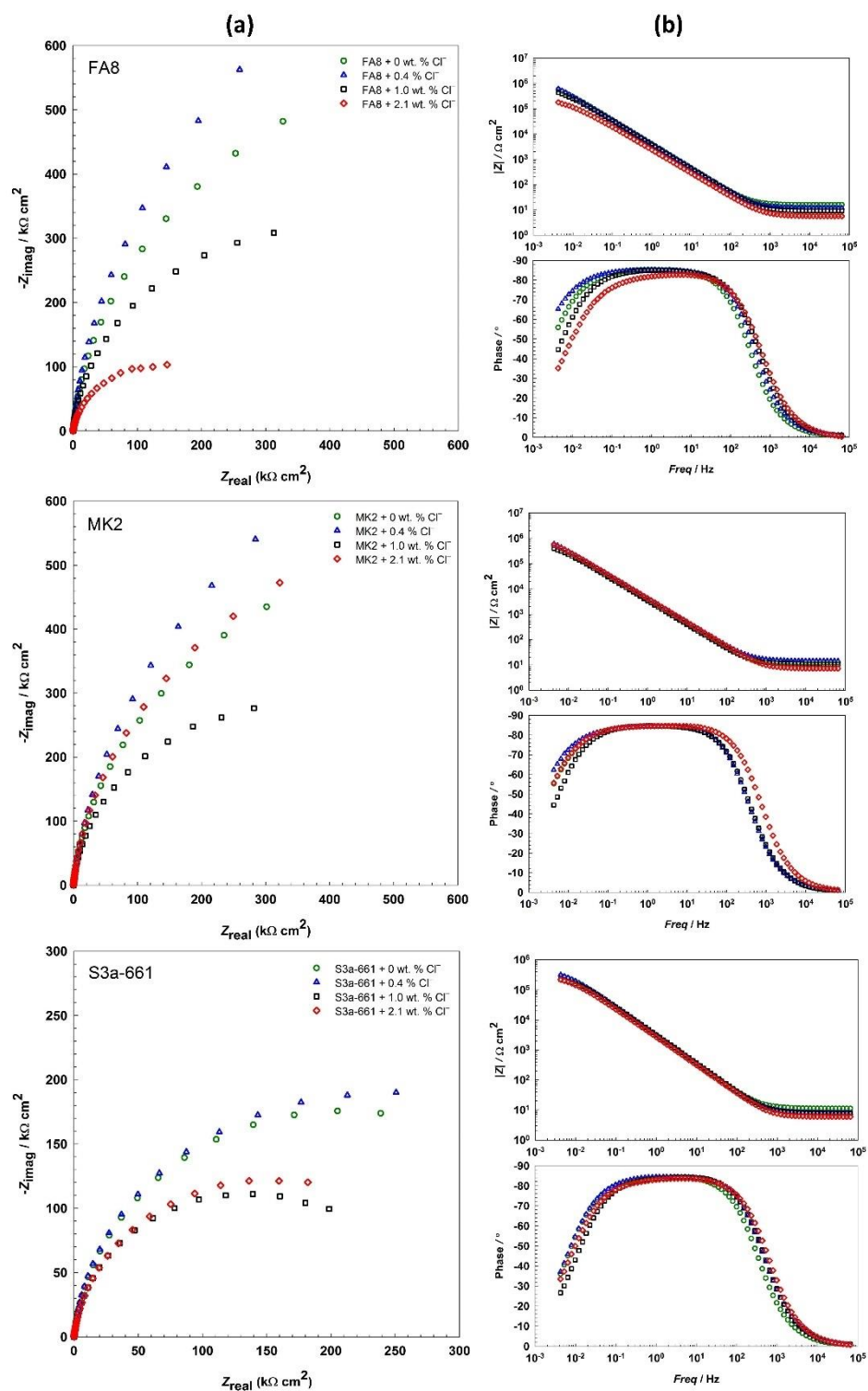


Figure 5. a) Nyquist EIS spectra and b) representative Bode EIS spectra measured in the three bare AAM pore solutions (Table 1) and those with added Cl^- at concentrations of 0.4 %, 1.0 % and 2.1 %.

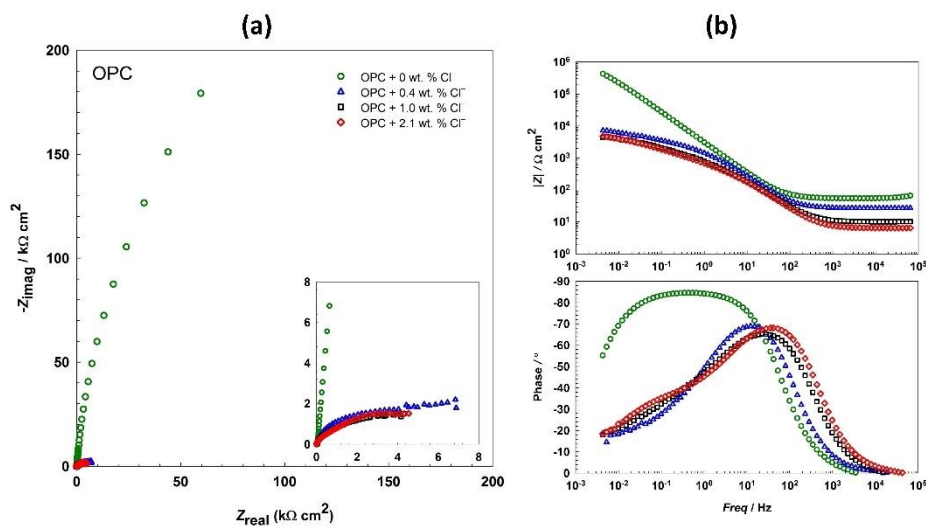


Figure 6. a) Nyquist EIS spectra and b) representative Bode EIS spectra measured in the bare OPC pore solution (0.031M NaOH) and the same solution with added Cl^- at concentrations of 0.4 %, 1.0 % and 2.1 %.

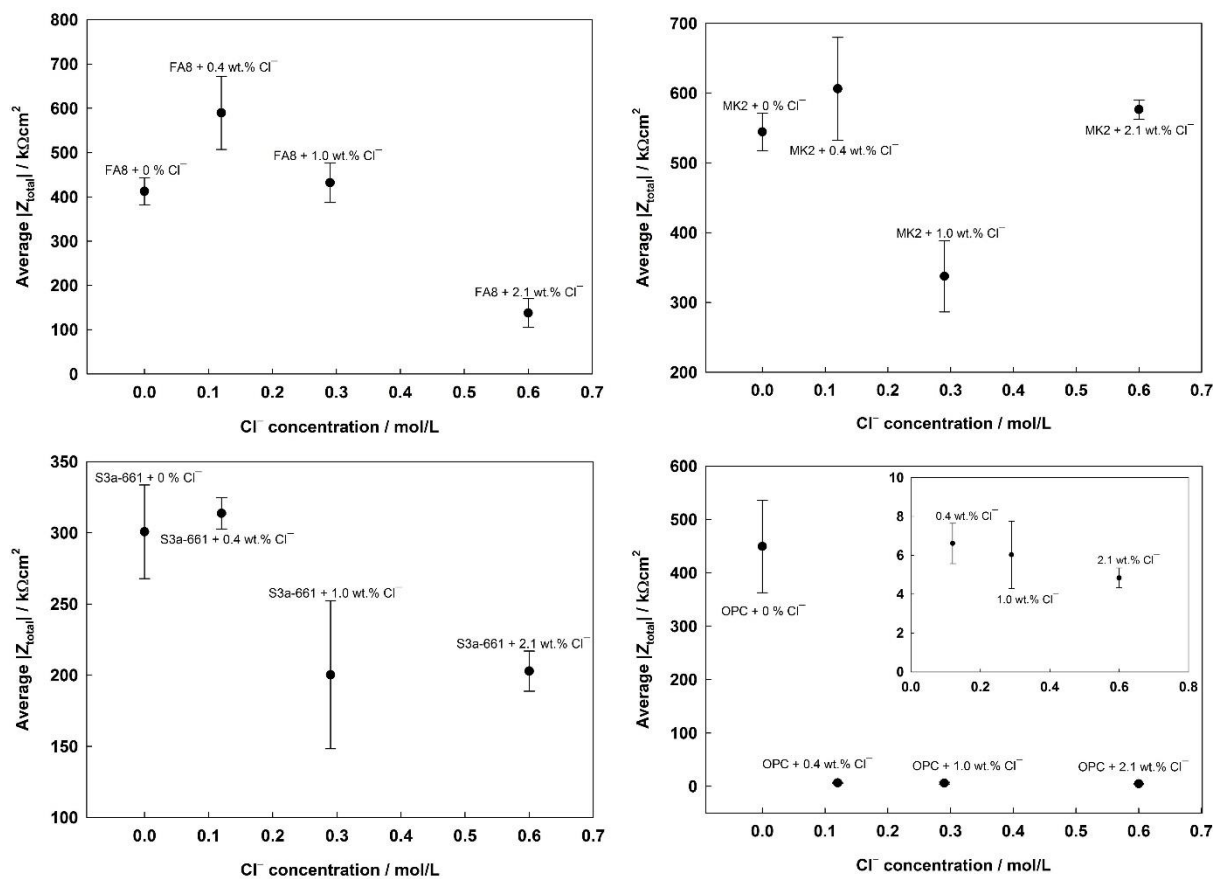


Figure 7. Average total impedance ($|Z_{total}|$) values at the lowest measured frequency in the three AAM pore solutions (Table 1), the OPC pore solution (0.031M NaOH), and the same solutions with the addition of Cl^- to concentrations of either 0.4 %, 1.0 % and 2.1 %.

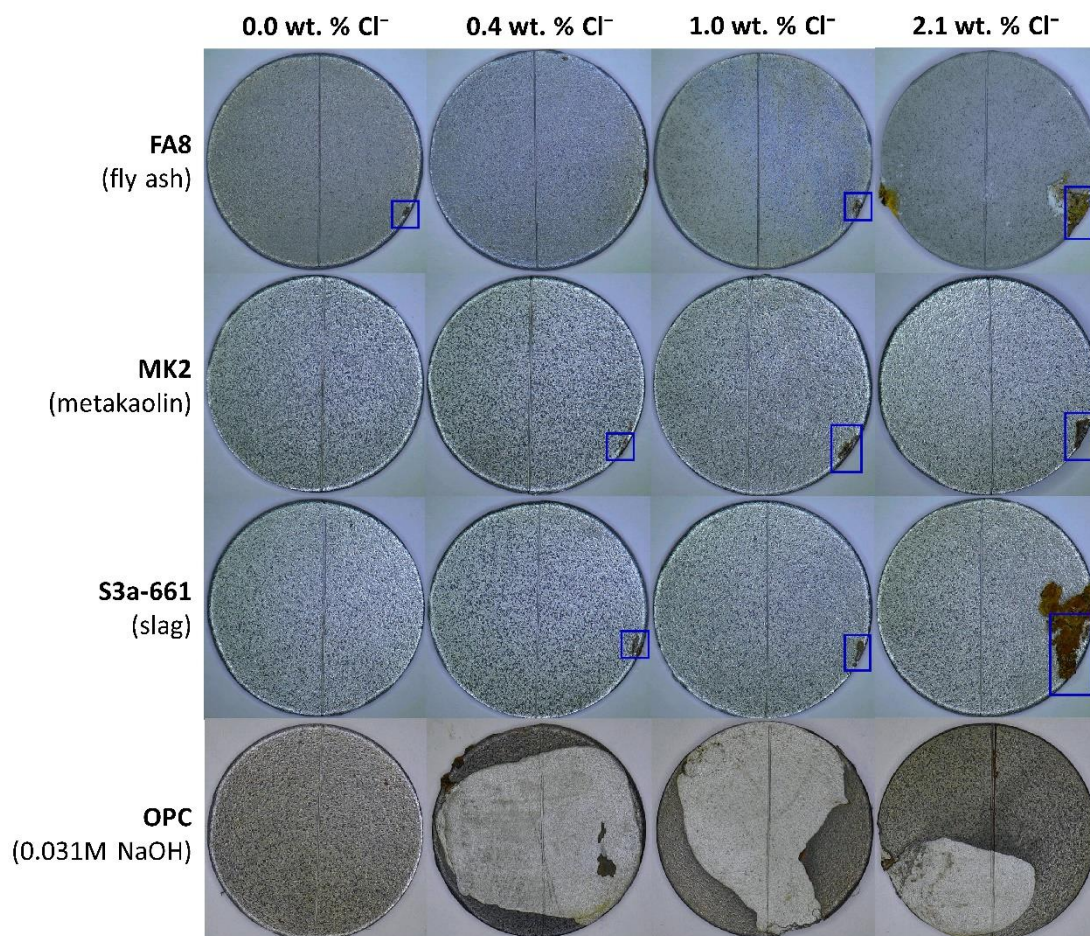


Figure 8. Visual analysis of the steel samples exposed to the three AAM pore solutions and the OPC pore solution (Table 1), both with and without the addition of Cl^- in various concentrations (0.4 %, 1.0 % and 2.1 %);  the blue rectangles indicate crevice corrosion at the point where the steel samples made contact with the Teflon holder.

TABLES

Table 1. Chemical compositions of the simulated pore solutions, prepared on the basis of analysis of the pore solutions extracted from the three alkali activated mortars (made from fly-ash (FA8), metakaolin (MK2) and steel slag (S3a-661)) [16].

Pore solution type	pH	Salts [g/L]									
		NaCl	KCl	K ₂ SO ₄	Na ₂ SO ₄	NaNO ₃	Na ₂ HPO ₄	NaOH	KOH	Na ₂ Si ₂ O ₅ (72 wt.%)	
AAM	FA8	12.4	0.053	-	1.502	22.871	-	7.859	2.081	-	79.968
	MK2	12.5	0.054	-	0.089	0.275	0.646	-	5.840	-	184.670
	S3a-661	12.7	-	0.400	0.914	-	-	-	1.430	1.805	196.486
OPC	12.8	-	-	-	-	-	-	-	1.240	-	-

Table 2. Chemical composition of the steel working electrode used for the electrochemical measurements.

Carbon (C)	Phosphorus (P)	Sulphur (S)	Copper (Cu)	Nitrogen (N)	Carbon Equivalent (C _{eq})
0.14 wt.%	0.008 wt.%	0.012 wt.%	0.073 wt.%	0.006 wt.%	0.23 wt.%

Table 3. Average corrosion rate (v_{corr}) values of steel in the various pore solutions (Table 1), both with and without the addition of Cl^- (to concentrations of 0.4 %, 1.0 % and 2.1 %), as calculated from parameters measured using three electrochemical techniques (LPR, CPD and EIS).

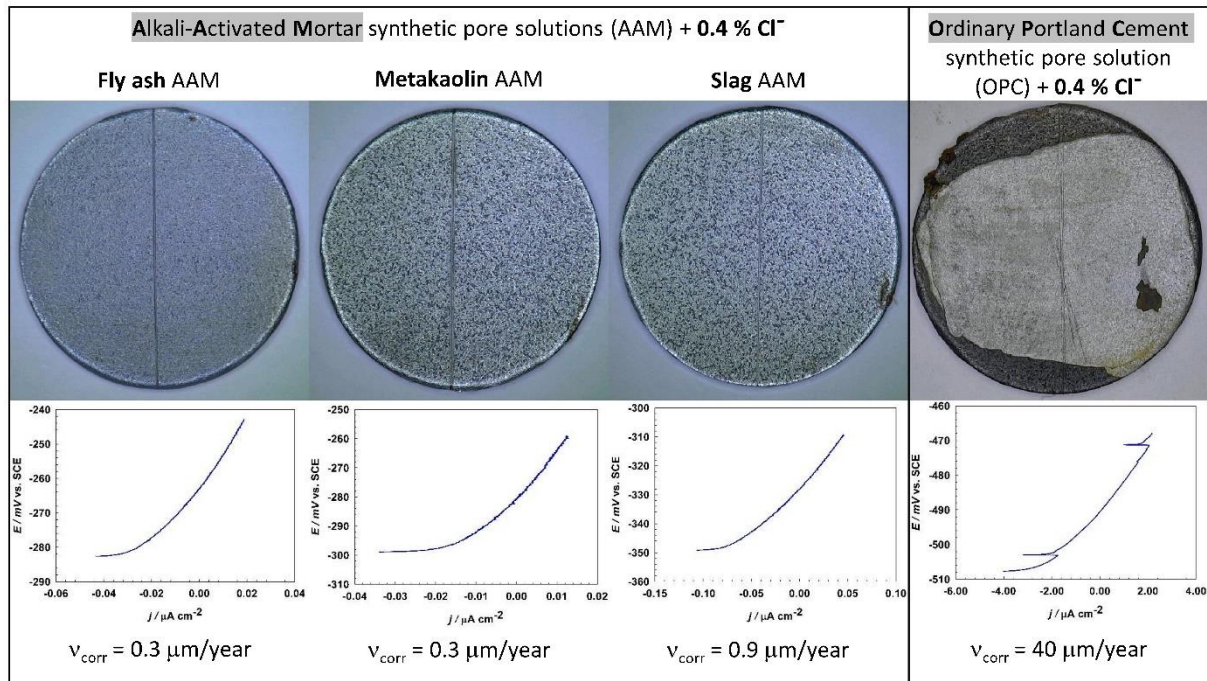
Method		LPR	CPD	EIS	
Pore solution type		v_{corr} [$\mu\text{m}/\text{year}$]	v_{corr} [$\mu\text{m}/\text{year}$]	v_{corr} [$\mu\text{m}/\text{year}$]	
0 (wt.) % Cl^-	AAM	FA8	0.5 ± 0.1	0.7 ± 0.1	0.7 ± 0.1
		MK2	0.3 ± 0.0	0.5 ± 0.1	0.6 ± 0.0
		S3a-661	0.9 ± 0.2	1.1 ± 0.3	1.0 ± 0.1
	OPC	0.031M NaOH	0.4 ± 0.1	0.4 ± 0.1	0.7 ± 0.1
0.4 (wt.) % Cl^-	AAM	FA8	0.3 ± 0.1	0.4 ± 0.1	0.5 ± 0.1
		MK2	0.3 ± 0.0	0.4 ± 0.1	0.5 ± 0.1
		S3a-661	0.9 ± 0.0	1.1 ± 0.1	1.0 ± 0.0
	OPC	0.031M NaOH	40 ± 5.9	53 ± 34	47 ± 8.0
1.0 (wt.) % Cl^-	AAM	FA8	0.5 ± 0.1	0.7 ± 0.1	0.7 ± 0.1
		MK2	0.8 ± 0.2	1.0 ± 0.1	0.9 ± 0.2
		S3a-661	1.6 ± 0.4	2.1 ± 0.7	1.6 ± 0.5
	OPC	0.031M NaOH	45 ± 14	38 ± 16	53 ± 15
2.1 (wt.) % Cl^-	AAM	FA8	2.5 ± 1.1	2.8 ± 1.1	2.3 ± 0.7
		MK2	0.3 ± 0.0	1.0 ± 0.8	0.5 ± 0.0
		S3a-661	1.3 ± 0.2	2.0 ± 0.4	1.5 ± 0.1

Method		LPR	CPD	EIS
Pore solution type		v_{corr} [$\mu\text{m}/\text{year}$]	v_{corr} [$\mu\text{m}/\text{year}$]	v_{corr} [$\mu\text{m}/\text{year}$]
OPC	0.031M NaOH	51 ± 4.8	32 ± 4.6	63 ± 6.6

Table 4. $\frac{[\text{Cl}^-]}{[\text{SO}_4^{2-}]}$ ratios in the pore solutions, taking into account both the existing (Table 1) and added Cl^- concentrations.

Pore solutions	PH	Added Cl^- concentrations			
		0.0 wt. % Cl^-	0.4 wt. % Cl^-	1.0 wt. % Cl^-	2.1 wt. % Cl^-
FA8	12.4	0.0053	0.712	1.715	3.54
MK2	12.5	0.377	49.3	118	245
S3a-661	12.7	1.023	23.9	56.3	115
OPC	12.8	-	-	-	-

GRAPHICAL ABSTRACT



Electrochemical techniques were used to study the corrosion of steel in pore solutions from different Alkali-Activated Mortars (AAMs) in the presence of Cl⁻. The results were compared to results measured in pore water simulating Portland cement (OPC) mortar. The important finding was that the corrosion processes on steel in the AAM simulated pore solutions are very different from processes of steel embedded in the AAM mortars, which was not the case for OPC.